Advances in Water Resources 105 (2017) 1–12

Contents lists available at ScienceDirect

Advances in Water Resources

journal homepage: www.elsevier.com/locate/advwatres

Development of a passive sensor for measuring vertical cumulative water and solute mass fluxes in lake sediments and streambeds

Leif Layton[a,b], Harald Klammler[a,b,*], Kirk Hatfield[a,b], Jaehyun Cho[a,b], Mark A. Newman[a,b], Michael D. Annable[a,b]

[a] Engineering School of Sustainable Infrastructure and Environment (ESSIE), University of Florida, Gainesville, FL 32611, USA
[b] Inter-Disciplinary Program in Hydrologic Sciences, University of Florida, Gainesville, FL 32611, USA

ARTICLE INFO

Article history:
Received 21 November 2016
Revised 29 March 2017
Accepted 21 April 2017
Available online 26 April 2017

Keywords:
Groundwater–surface water interaction
Hyporheic and hypolentic zones
Passive flux meter
Vertical flow
Contaminant transport
Water flux
Mass flux

ABSTRACT

This paper introduces the sediment bed passive flux meter (SBPFM) as a new tool for in situ measurements of vertical volumetric water and contaminant mass fluxes across hyporheic and hypolentic zones (i.e., stream or lake bed sediments that function as the contiguous zone between the overlying surface water body and the underlying aquifer). The device is a direct-push probe which contains a permeable internal sorbent located between two screened intervals. In the presence of a vertical hydraulic gradient the screens allow water flow through the SBPFM's internal sorbent matrix that is impregnated with resident tracers. These tracers are displaced from the sorbent at rates proportional to the water flux through the sorbent. At the same time, dissolved contaminants present in the intercepted sediment water are retained on the SBPFM sorbent at rates proportional to the ambient contaminant mass flux in the hyporheic zone. Potential flow theory is applied to convert observations of water and contaminant fluxes through the SBPFM into estimates of undisturbed ambient vertical water and contaminant fluxes in the sediment. To validate the theory and demonstrate the SBPFM as a potential site characterization tool, multiple bench-scale sediment bed experiments are performed. Results demonstrate that water and contaminant mass fluxes are accurately measured in the laboratory and that future field tests are warranted.

1. Introduction

The contamination of both ground and surface water bodies has become a growing concern worldwide (Kalbus et al., 2006). Traditionally, aquifers and streams have been treated and managed separately from one another (Constantz et al., 2001; Winter et al., 1998); however, in the last few decades this paradigm has shifted to an understanding that rivers and aquifers do not exist as separable entities (Winter, 2001). As a consequence, groundwater–surface water interactions and the hydrodynamic processes controlling these interactions have received considerable attention at various scales (Sawyer et al., 2014; Boano et al., 2007; Constantz et al., 2001; Packman & Salehin, 2003; Rosenberry, 2008; Winter et al., 1998).

Understanding of groundwater–surface water interaction is essential for the effective management of both water quality and quantity issues (Constantz et al., 2001). This involves processes controlling water and contaminant transport and biogeochemical reactions in the hyporheic and hypolentic zones (i.e., stream or lake bed sediments that function as the contiguous zone between the overlying surface water body and the underlying aquifer; Winter, 2001). These processes and reactions are challenging to measure within the sediment at the local scale and are difficult to interpret at larger stream and lake scales (Baxter et al., 2003; Boulton et al., 1998). Methods currently available to assess solute and water interactions as well as exchange at the sediment–water interface are based on measurements of different types of parameters (e.g., temperatures, gradients, concentrations, etc.) rendering, hence, results vulnerable to different types of erroneous interpretation (Belanger & Montgomery, 1992; Brodie et al., 2009).

Perhaps the most well-known method is the seepage meter, which provides direct measurements of seepage flux at the water–sediment bed interface (i.e., not within the hyporheic or hypolentic zones). The device requires little to no experience to deploy, is relatively simple and inexpensive to build and operate, and requires no knowledge of the local hydraulic gradient or permeability of bed sediments. In addition, because it captures water from the underlying contiguous aquifer in a plastic bag, chemical analysis for the target contaminants in that water can yield estimates of con-

* Corresponding author at: Engineering School of Sustainable Infrastructure and Environment (ESSIE), University of Florida, Gainesville, FL 32611, USA.
E-mail addresses: haki@gmx.at, haki@ufl.edu (H. Klammler).

http://dx.doi.org/10.1016/j.advwatres.2017.04.018
0309-1708/

List of variables

A_S	Horizontal area of interest for discharge estimation
B_n	Constants in SBPFM flow field solution
F_{open}	Shape factor corresponding to "open" SBPFM (infinite K_c)
F_{rec}	Shape factor corresponding to recirculating flow between SBPFM screens
I_i	Modified Bessel function of the first kind and ith order
J	Undisturbed vertical hydraulic gradient in sediment bed
J_C	Undisturbed vertical contaminant mass flux in the sediment bed
J_i	Bessel function of the first kind and ith order
K	Hydraulic conductivity of sediment bed under isotropic conditions
K_c	Hydraulic conductivity of the SBPFM sorbent
K_H	Horizontal hydraulic conductivity of the sediment bed
K_i	Modified Bessel function of the second kind and ith order
K_V	Vertical hydraulic conductivity of the sediment bed
L	Length of rectangular sediment box for direct testing of K_H
L_c	Length of the sorbent column
$L_{1,2}$	Distances between sediment surface and lower end of conductivity test pipe
M_Q	Contaminant mass flow (discharge)
N	Number of terms in summation of SBPFM flow field solution
Q	Flow through rectangular sediment box for direct testing of K_H
Q_c	Water discharge through sorbent column
Q_{inj}	Injection flow (discharge) during injection through both screens in the bucket
Q_{open}	Water discharge though SBPFM without sorbent (infinite K_c)
Q_{rec}	Water discharge between SBPFM screens for (hypothetical) recirculation
Q_{sim}	Vertical water discharge through sand bucket with SBPFM installed
$Q_{1,2}$	Injection flows for measuring K_V using injection through pipe
$Q_{V,VII}$	Water discharges through bottom and top screens
R_d	Retardation factor of a resident tracer W ... Width of rectangular sediment box for direct testing of K_H
Y_i	Bessel function of the second kind and ith order
a	Outer SBPFM radius
b	Radial extent of flow domain
c_F	Flux-averaged contaminant concentration
c_0	Initial aqueous resident tracer concentration in the sorbent
$c_{1\text{-}12}$	Real constants in general flow field solution
d	Distance between upper and lower boundaries
d_{bot}	Distance between bottom boundary and lower SBPFM screen
d_{top}	Distance between sediment surface and upper SBPFM screen
dA	Infinitessimal area for integration of fluxes to discharge
f_0	Auxiliary function in SBPFM flow field solution
$h_{1,2,3,4}$	Vertical coordinates of screen limits
i, j	Auxiliary variables
m_C	Mass of contaminant sorbed
m_I	Initial tracer mass on the sorbent
m_L	Tracer mass lost from the sorbent due to water flow
m_R	Resident tracer mass remaining on the sorbent
$m_{1\text{-}4}$	Positive real constants in general flow field solution
m, n	Auxiliary variables in SBPFM flow field solution
q_c	Water flux through the sorbent column
q_{sim}	Average vertical water flux through sand bucket with SBPFM installed
q_0	Undisturbed vertical volumetric water flux in the sediment bed
p	Length of impermeable casing between screens
r	Radial coordinate
r_c	Radius of the sorbent column
s	Screen length
t	SBPFM test duration
z	Vertical coordinate
z_i	Vertical coordinates of control points along SBPFM surface
$\Delta\phi$	Head difference across sorbent column
Δt	Time intervals for falling head test
Ω_R	Relative remaining tracer mass
α_q	Flow convergence coefficient
ϕ	Hydraulic head in sediment bed
ϕ_{inj}	Injection head during injection through both screens in the bucket
$\phi_{0,L}$	Entrance and exit heads in rectangular sediment box for direct testing of K_H
$\phi_{1,2}$	Injection heads for measuring K_V using injection through pipe
$\phi_{II,III}$	Hydraulic heads at top and bottom boundaries
$\phi_{V,VII}$	Hydraulic heads at bottom and top screens
ρ	Anisotropy ratio in sediment conductivity
θ	Saturated water content of sorbent

taminant fluxes across ground–surface water interfaces (Kalbus et al., 2006; Lee, 1977; Rosenberry, 2008). However, it may be susceptible to multiple sources of error, such as channeling effects due to incorrect installation, release of interstitial gasses upon installation, Venturi effects and deformation due to stream flow around the collection bag, and unaccounted hydraulic head losses (Russoniello and Michael, 2014; Brodie et al., 2009; Lee, 1977; Murdoch and Kelly, 2003; Rosenberry and Morin, 2004; Taniguchi and Fukuo, 1993).

To the best of our knowledge, there is no passive monitoring tool that provides simultaneous measurements of water and contaminant fluxes in both losing and gaining streams and lakes. Contaminant mass flux is generally determined as the product of the pore water concentration within the sediment bed and Darcy flux across the sediment–water interface. Pore water concentration may be measured from core samples, but in situ techniques are preferred as they introduce less potential for contamination of the water sample (Bufflap and Allen, 1995). Pump tests may be used to measure pore water concentrations and provide integral measurements that are less susceptible to heterogeneity effects of the subsurface and contaminant distribution than point measurements. However, those require the disposal of large volumes of contaminated groundwater and application near streams may cause problems resulting from the influence of pumped stream water. Alternatively, samples from (multi-level) piezometers or sampling wells closely spaced and aligned in transects can provide very detailed information about contaminant distributions (Kalbus et al., 2006).

Passive samplers offer an attractive alternative to pore water samples, because they collect the target analytes in situ and without affecting the bulk solution. Moreover, they can be used

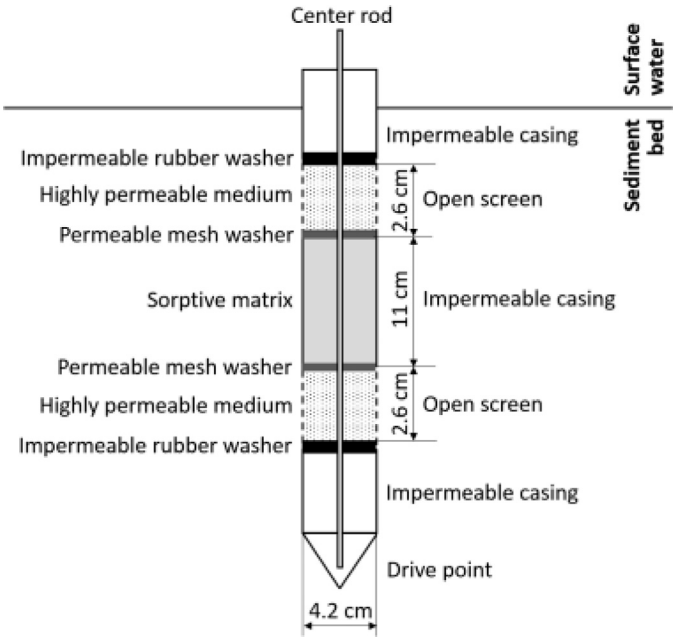

Fig. 1. Schematic of the sediment bed passive flux meter (SBPFM; not to scale) with dimensions used in laboratory experiments.

for a wide range of chemical constituents and are able to detect low contaminant concentrations (Ghosh et al., 2014; Kalbus et al., 2006; Vrana et al., 2005). They are simple, relatively inexpensive, require no additional equipment or power, and may be left unattended during operation, thus offering time and cost efficient results without sacrificing data quality. Furthermore, passive devices provide time-averaged measurements, which are less sensitive to daily fluctuations due to accumulation of contaminants over the entire sampling period (Kalbus et al., 2006). Passive samplers currently used to measure pore–water concentrations in sediment beds include dialysis samplers, dialysis bags, and devices employing a diffusive equilibrium in a thin film (e.g., Ghosh et al., 2014; Bufflap and Allen, 1995).

The purpose of this paper is to introduce a new passive monitoring device called the sediment bed passive flux meter (SBPFM). We establish its theoretical foundation, provide a proof of concept through laboratory sand bucket experiments and discuss different aspects toward its practical application, including inherent limitations. The SBPFM is capable of providing in situ point measurements of vertical water flux q_0 [LT^{-1}] and contaminant mass flux J_C [$ML^{-2}T^{-1}$] through sediment beds of lakes and streams. Contaminant mass flow (discharge) may then be estimated from spatially interpolating and integrating point measurements of J_C as

$$M_Q = \int_{A_s} J_C dA = \int_{A_s} q_0 c_F dA \tag{1}$$

where M_Q [MT^{-1}] is the mass flow rate of a contaminant over horizontal area A_s [L^2], and c_F [ML^{-3}] is the flux-averaged concentration of the contaminant. In the following section, we present a typical SBPFM design and the underlying concept for acquiring measurements of vertical fluxes through sediment beds. Subsequent sections contain the necessary theoretical development end experimental design, before analyzing and discussing results.

2. Sediment bed passive flux meter (SBPFM) concept and design

The SBPFM is a direct-push probe with two screened intervals (Fig. 1). The device is driven directly into the uppermost sediment layers of stream and lake beds to remain for a period of time (e.g., from hours to weeks). Subjected to the ambient vertical hydraulic gradient, groundwater enters the SBPFM through one screen and exits through the other. Thus, the SBPFM passively intercepts water and contaminants flowing vertically through the sediment. Between the screens, the SBPFM contains a permeable sorbent impregnated with one or more fluid–soluble resident tracers (e.g., alcohols), which are eluted at rates proportional to the fluid flux. After a designated deployment period, the SBPFM is removed and the sorbent is carefully extracted to quantify the residual mass of the impregnated resident tracers for calculation of the cumulative water flux through the sorbent. Simultaneously, the masses of all contaminants intercepted and retained on the sorbent are quantified to calculate cumulative contaminant mass fluxes through the sorbent. Details about the measurement of water and contaminant mass fluxes through the sorbent, and subsequent conversion to undisturbed ambient fluxes in the sediment are described in detail below.

3. Methods

3.1. Theory

3.1.1. Water flux

Initially, each resident tracer is uniformly distributed over the column of sorptive matrix within the SBPFM. After installation and during a period of exposure to local sediment bed water fluxes, the tracers are displaced from the SBPFM. The residual mass of resident tracer remaining on the sorbent matrix m_R [M] is the difference of the initial mass equilibrated on the sorbent matrix m_I [M] and the mass eluted from the matrix due to groundwater flow through the device m_L [M]. It may be expressed as

$$m_R = m_I - m_L \tag{2}$$

The residual mass of the resident tracer on the sorbent is inversely proportional to the cumulative volume of water that has been intercepted by the sorbent; therefore, the cumulative or time-averaged water flux can be estimated from measurements of m_R.

The relationship between m_R and the flux through the sorbent column q_c [LT^{-1}] can be derived by defining the mass fraction of initial tracer remaining on the sorptive matrix Ω_R [-] after exposure to water flow for a period t [T] as

$$\Omega_R = \frac{m_R}{m_I} \tag{3}$$

The initial mass of the resident tracer impregnated on the sorptive matrix is calculated as

$$m_I = \pi r_c^2 L_c \theta R_d c_0 \tag{4}$$

where r_c [L] and L_c [L] are the radius and length of the sorbent column in the SBPFM, respectively, θ [-] is the saturated water content of the sorbent, R_d [-] is the retardation factor of a resident tracer, and c_0 [ML^{-3}] is the initial aqueous resident tracer concentration in the pore space. Following Hatfield et al. (2004) we assume that tracer transport is primarily advective and that tracer sorption is linear, reversible, and instantaneous. Thus, the mass eluded from the sorptive matrix is equal to

$$m_L = \pi r_c^2 q_c t c_0 \tag{5}$$

and we can express Ω_R by combining equations (2) – (5) as

$$\Omega_R = 1 - \frac{q_c t}{L_c \theta R_d} \tag{6}$$

The undisturbed time-averaged specific discharge through the sediment bed q_0 can be found from the relationship

$$q_c = \alpha_q q_0 \tag{7}$$

where α_q [-] is a flow convergence coefficient characterizing the distortion of the otherwise uniform flow of water through the sediment bed due to the presence of the SBPFM. Finally, Eqs. (6) and (7) combine to form

$$q_0 = \frac{(1-\Omega_R)L_c\theta R_d}{\alpha_q t} \tag{8}$$

Estimates of q_0 have decreased accuracy as the value of Ω_R approaches either 1 or 0 (Hatfield et al., 2004). Thus, under conditions where no prior estimates of sediment bed water flux exist, the use of multiple resident tracers with varying retardation factors increases the likelihood that one or more resident tracers will be in an intermediate range of Ω_R.

3.1.2. Contaminant flux

Measurement of contaminant flux is performed by quantifying the masses of target dissolved contaminants in the sediment bed water, which are intercepted and retained by the SBPFM sorbent. The contaminant mass flux of any dissolved organic or inorganic contaminant can be measured if (1) the sorbent of the SBPFM intercepts and fully retains the contaminant from the water flowing vertically in the sediment bed, if (2) the contaminant can be extracted from the sorbent or analyzed in the sorbed state, such that the mass of the contaminant retained can be measured, and if (3) the contaminant does not degrade inside the SBPFM between interception and extraction. Contaminant mass flux through the SBPFM is equal to the mass of contaminant sorbed m_C [M] per unit cross-sectional area and per unit time. From Eq. (7) it can be inferred that ambient contaminant flux through the sediment J_C and the contaminant mass flux through the SBPFM differ by a factor α_q, leading to

$$J_C = \frac{m_C}{\alpha_q \pi r_c^2 t} \tag{9}$$

In order to make use of Eqs. (8) and (9), the remaining problem is the quantification of the flow convergence coefficient α_q.

3.1.3. Flow convergence

The flow convergence coefficient α_q for the SBPFM is a function of the geometric and hydraulic properties of the probe, the sorbent column and the surrounding sediment. As derived in detail in Appendix A, a convenient method of computing α_q for an anisotropic sediment of hydraulic conductivities K_H and K_V [LT^{-1}] in the horizontal and vertical directions, respectively, is

$$\alpha_q = \frac{F_{open}}{\left(\frac{r_c}{a}\right)^2 + \frac{L_c K_V}{(p+s)K_c} F_{rec}} \tag{10}$$

where a [L] is the outer probe radius, p [L] is the length of impermeable casing between the two screens, s [L] is the length of each screen, and r_c [L], L_c [L] and K_c [LT^{-1}] are radius, length and hydraulic conductivity of the sorbent column. F_{open} [-] and F_{rec} [-] are constants that depend on both the geometry of the SBPFM and the flow domain and are determined following the method of Klammler et al. (2011) as described in Appendix B. For a range of typical field conditions, F_{open} and F_{rec} can be graphically represented (Figs. 2 and 3), where the anisotropy ratio ρ [-] is defined as

$$\rho^2 = \frac{K_V}{K_H} \tag{11}$$

For future field applications it is expected that $p/s \geq 1$ is the case, for which $F_{rec} = F_{open}$ is an acceptable approximation to be used in Eq. (10) (Fig. 3).

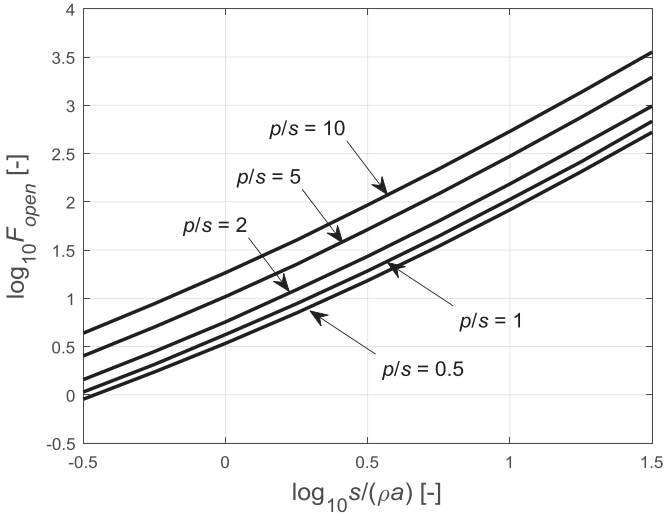

Fig. 2. $\log_{10}(F_{open})$ as a function of p/s and $\log_{10}s/(\rho a)$ for computation of α_q from Eq. (10) under field conditions (sediment bed of anisotropy ratio ρ and distant bottom/lateral boundaries; see Appendix B1 for derivation). SBPFM geometry is described by radius a, screen length s and distance p between screens.

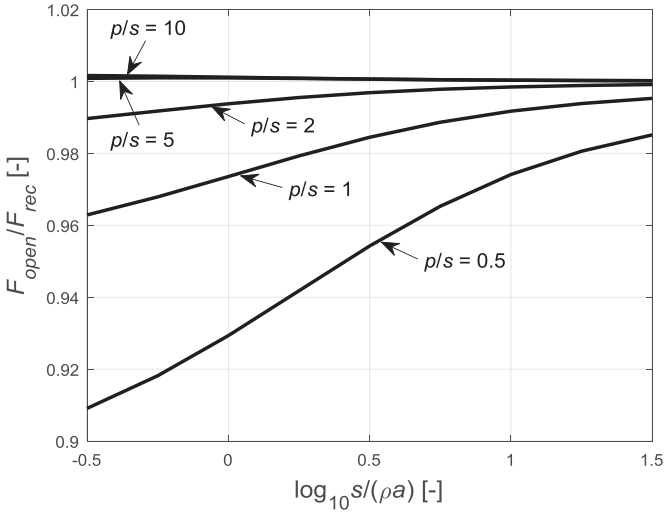

Fig. 3. F_{open}/F_{rec} as a function of p/s and $\log_{10}s/(\rho a)$ for computation of α_q from Eq. (10) under field conditions (see Appendix B2 for derivation).

3.1.4. Sediment conductivity (field application)

Quantification of the flow convergence factor α_q from Eq. (10) requires knowledge of anisotropy ratio ρ (for determining F_{open} and F_{rec} from Figs. 2 and 3) and vertical sediment conductivity K_V. This may be achieved by one of the methods proposed by Klammler et al. (under review in AWR as manuscript ADWR_2016_360_R1). Moreover, a contour plot of α_q as a function of K_c/K_V and K_V/K_H on log-log scale may be generated for an exemplary field scenario (Fig. 4). This plot immediately illustrates the degree of sensitivity (variability) of α_q and, hence, resulting water and contaminant mass flux estimates, over regions delimited by upper and lower uncertainty bounds in K_V and K_V/K_H, for example. Inside the shade rectangle, the contour lines are essentially vertical, indicating minimal sensitivity of α_q to K_H. The rectangle spans the region of $K_V \leq K_H$, which is typical for sediment deposits, and $K_c \leq 10K_V$, which is approximately equivalent to limiting $\alpha_q \leq 10$ for avoiding unnecessarily large distortions of the ambient flow field near the SBPFM.

Consequently, α_q may be reliably inferred from knowing K_V only, for which we propose a measurement technique based on in-

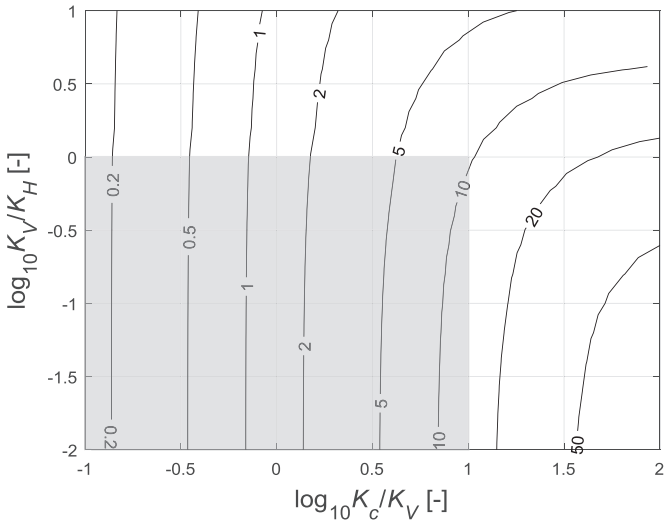

Fig. 4. Contour lines of α_q as a function of $\log_{10}K_c/K_V$ and $\log_{10}K_V/K_H$ for exemplary field conditions (i.e., distant lateral and bottom boundaries), $d_{top}=10$ cm, $a=2$ cm, $s=4$ cm, $p=L_c=10$ cm and $r_c=1.5$ cm. The shaded rectangle indicates region of minimal sensitivity of α_q to K_H.

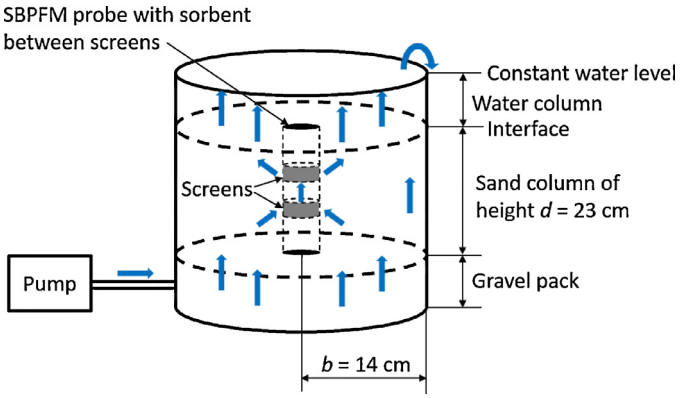

Fig. 5. Schematic sketch of laboratory experiments using sediment bed simulator consisting of a bucket packed with gravel and sand. Blue arrows indicate local directions of water flow. (For interpretation of the references to color in this figure legend, the reader is referred to the web version of this article.)

jection through the bottom of a hollow pipe inserted into the sediment bed. Hvorslev (1951; Fig. 12, case 6) provides a relationship between injection head ϕ_1 and flow rate Q_1 for this test, which can be written as

$$\frac{\phi_1}{Q_1}=\frac{1}{5.5a\rho K_H}+\frac{L_1}{a^2\rho^2\pi K_H} \tag{12}$$

where L_1 [m] is the distance the pipe is inserted into the sediment. Eq. (12) is obtained from Hvorslev's equation after scaling the flow domain to isotropy through multiplying all radial coordinates by ρ and using an isotropic effective conductivity equal to K_H (Hvorslev, 1951). The first term on the right-hand-side corresponds to the resistance to flow after leaving the pipe. The last term represents Darcy's law for the almost perfectly vertical flow through the sediment column inside the pipe of $K_V=\rho^2K_H$. The same applies for a second injection test after advancing the pipe tip to a larger depth L_2 into the sediment.

$$\frac{\phi_2}{Q_2}=\frac{1}{5.5a\rho K_H}+\frac{L_2}{a^2\rho^2\pi K_H} \tag{13}$$

Subtracting Eq. (12) from Eq. (13) and using $K_V=\rho^2K_H$ gives

$$K_V=\frac{L_2-L_1}{a^2\pi\left(\frac{\phi_2}{Q_2}-\frac{\phi_1}{Q_1}\right)} \tag{14}$$

for estimating K_V. Intuitively speaking, by taking the difference, the influence of the flow field after leaving the pipe tip is eliminated and what is left is the effect of the (almost) perfectly vertical flow through the sediment inside the pipe. Eq. (14) is formulated in terms of constant head/steady-state injection tests, but may be easily converted to be applied with falling head/slug tests using (Hvorslev, 1951)

$$a^2\pi\frac{\phi_j}{Q_j}=\frac{\Delta t}{\Delta ln\phi_j} \tag{15}$$

for both injection tests ($j=1, 2$), where the right-hand-side is simply the inverse slope of the log-head over time data points.

3.2. Experimental design

3.2.1. Sediment bed simulator

Bench scale sediment bed laboratory experiments were conducted to evaluate the SBPFM. These involved installing the device in a constructed sediment bed simulator, in which controlled water and contaminant mass fluxes could be established. The simulator was built using a bucket of 36.4 cm in height and $b=14$ cm in radius (Fig. 5). The bottom 4 cm of the bucket was packed with coarse gravel to ensure water entering through an installed fitting at the bottom of the bucket had a constant head across the horizontal cross-section of the bucket. A PVC pipe of inner diameter $r_c=1.7$ cm and outer diameter $a=2.1$ cm was used as the casing of the SBPFM and positioned upright in the center of the bucket. Two slotted sections of length $s=2.6$ cm served as screens to allow flow into and out of the device and were separated by an impermeable portion of length $p=11$ cm. The distance between bottom screen and bottom boundary was $d_{bot}=3.6$ cm and that between top screen and top boundary was $d_{top}=3.3$ cm.

To avoid channeling effects associated with shifting of the casing in the sand during installation of the sorbent, the casing was held in place by a PVC adaptor fixed to the walls of the bucket by threaded steel rods. Medium to fine commercial grade sand was packed around the casing under standing water to a height of approximately $d=23$ cm with approximately 2–3 cm of standing water above the top of the sand. Water was pumped into the gravel at the bottom of the bucket by a peristaltic pump at flow rates ranging from 0.36–6.46 L/h giving a uniform ambient specific discharge of $q_0=14$–242 cm/d with closed screens.

2-octanol served as a surrogate contaminant in the water flowing through the sediment. Preceding experiments, in which contaminant mass flux was measured, 5 pore volumes of the desired concentration of a 2-octanol and water solution were flushed through the sediment bed simulator, while the screens of the installed casing were closed, to create a uniform initial concentration distribution in the sediment. The 2-octanol solution was prepared prior to the experiments and 2-octanol influent concentrations ranged from 2 to 39 mg/L. Influent and effluent samples were taken periodically throughout the experiments for subsequent analysis.

3.2.2. Sediment conductivity and flow convergence (laboratory experiments)

For calculation of the convergence factor α_q using Eq. (10), we determined $K_V=68.5$ m/d from a constant head permeability tests with closed SBPFM screens. This test imposed uniform vertical flow across the sand column between top and bottom boundaries and allowed for direct application of Darcy's law. In order to obtain additional information to determine the horizontal conductivity K_H, the screens were opened for an injection test. Water was pumped through both SBPFM screens at a constant rate and allowed to exit

the sediment bed simulator through the top and bottom boundaries (both connected to the same constant head reservoir). The pumping rate and the injection head were recorded at steady-state. These two values were used in combination with K_V to determine $\rho = 0.8$ using the method described in Appendix C and, subsequently, $K_H = 113$ m/d from Eq. (11).

This result was further verified through independent testing of the horizontal hydraulic conductivity. The sediment was packed similarly under standing water in a small rectangular box aquifer with gravel packed at two opposite walls serving as inlet and outlet. Both were connected to a constant head reservoir that created a horizontal hydraulic gradient across the sediment in the box. The horizontal hydraulic conductivity was calculated as $K_H = 2LQ/[W(\phi_0{}^2 - \phi_L{}^2)]$, where L [L] is the length of the sediment in the direction of travel, W [L] is the width, Q [L^3T^{-1}] is the volumetric flow rate through the sediment, ϕ_0 [L] is the height of the water at the inlet, and ϕ_L [L] is the height of the water at the outlet (Bear, 2013). The horizontal hydraulic conductivity determined from these tests was $K_H = 112$ m/d.

For the given bucket and probe geometries, equations (B23) and (B26) from Appendix B deliver $F_{open} \approx F_{rec} \approx 17.5$. With sorbent column lengths for a first set of experiments ranging from $L_c = 6.4$–7.2 cm, this led to flow convergence factors $\alpha_q = 6$–6.7 as determined by Eq. (10). For a second set of experiments (those involving contaminant mass flux), the simulator was drained and packed again, and hydraulic conductivities were found to be $K_H = 158$ m/d and $K_V = 101$ m/d. For these experiments the length of sorbent ranged from $L_c = 7.0$–7.4 cm and the resulting flow convergence factors were calculated as $\alpha_q = 4.2$–4.5.

3.2.3. Preparation of the SBPFM

The sorbent used in the SBPFMs consisted of silver-impregnated (0.2%) granular activated carbon (GAC), which was manually packed into fine-meshed nylon socks inside a transparent casing. The socks were 30 cm long with a diameter of 3.5 cm ($\approx 2r_c$) and built around a stainless steel rod with a diameter of 0.7 cm (Fig. 1). Each sock was packed with approximately 35 g (dry mass) of GAC, resulting in sorbent columns of $L_c = 6.5$– 7.5 cm in length. Above and below the activated carbon the SBPFM was filled with 0.3 cm diameter glass beads of large bulk hydraulic conductivity. Glass beads and activated carbon were separated by mesh washers while rubber washers confined the outer most portions of the glass beads within the SBPFM. The activated carbon had a hydraulic conductivity of $K_c = 300$ m/d, a saturated water content of $\theta = 0.55$, and a dry bulk density of 0.5 g/cm^3.

The resident tracers applied on the sorbent were methanol, ethanol, 2-propanol, tert-butanol, and 2,4-dimethyl-3-pentanol. Prior to installation, these tracers were pre-equilibrated on the activated carbon by gently mixing the carbon for 24 h in an aqueous solution containing methanol, ethanol, and 2,4-dimethyl-3-pentanol at a concentration of $c_0 = 1200$ mg/L, and 2-propanol and tert-butanol at a concentration of $c_0 = 2300$ mg/L. Tracer impregnated activated carbon sorbent was drained before packing into the sock along with the glass beads. The packed sock was then transferred from the transparent casing into the screened casing installed in the sediment bed simulator. During the construction of each SBPFM a portion of the GAC was sampled to establish initial concentration of the resident tracers used to calculate Ω_R.

Independent of the sediment bed simulator, column elution experiments were conducted with the same tracer-equilibrated activated carbon packed in flow-through columns. The tracer concentrations in flow-through column effluents were monitored to obtain Ω_R, which was subsequently plotted as a function of pore volumes conveyed through the column. The elution curves were then used to determine the range of $\Omega_R > 0.3$, over which elution was linear (Hatfield et al., 2004). The retardation factor for each tracer was found by taking the inverse of the slope of the linear portion of each curve (Table 1).

Table 1
Retardation factors of resident tracers as determined from independent column elution experiments.

Resident tracer	Retardation factor R_d
Methanol	5
Ethanol	27
2-propanol	120
Tert-butanol	295
2,4-dimethyl-3-pentanol	>10,000

3.2.4. Sorbent analysis

After the desired duration of deployment, ranging from 1.4–115.8 h, the SBPFM sorbent was pulled, well mixed and sampled. Resident tracers and contaminant surrogate were extracted from the GAC using isobutyl alcohol. Using extraction efficiencies determined from independent batch tests, all samples were analyzed for tracer and contaminant masses on a Perkin–Elmer gas chromatograph equipped with automated liquid injection and a flame ionization detector. Because the retardation factor of 2,4-dimethyl-3-pentanol is in excess of 10,000 at the concentration used during experiments, it is used as an internal standard such that changes in the residual mass of the other resident tracers were evaluated from measured changes in tracer mass ratios with respect to 2,4-dimethyl-3-pentanol. Computing Ω_R in this manner assumes that any loss of mass of 2,4-dimethyl-3-pentanol is due to some unaccounted source(s) of error that also increased mass loss of the other resident tracers, which needs to be compensated for (Hatfield et al., 2004). Thus, Ω_R for each resident tracer was calculated as

$$\Omega_R = \frac{m_R/m_{R,DMP}}{m_I/m_{I,DMP}} \tag{16}$$

where $m_{R,DMP}$ [M] and $m_{I,DMP}$ [M] are the residual and initial masses, respectively, of 2,4-dimethyl-3-pentanol on the activated carbon for each experiment. Measured values of Ω_R for each resident tracer were used in Eq. (8) to estimate water fluxes q_0 for comparison to the known water fluxes imposed through the SBPFM. Similarly, measured values of sorbed contaminant mass m_C are used to estimate contaminant mass fluxes J_C from Eq. (9). See Appendix B3 for further details related to the calculation of true water and contaminant fluxes in the sediment bed simulator.

4. Results and discussion

4.1. Installation losses and general tracer performance

Because the design of the SBPFM permits vertical flow, the vertical installation and retrieval of the sorbent inevitably forced portions of the water through the sorbent and resulted in excess tracer elution. To quantify the impact of installation and retrieval on tracer elution, a test was performed in which the SBPFM was deployed and immediately retrieved from the sediment bed simulator. While losses were negligible for 2-propanol and tert-butanol, mass loss was evident in methanol and ethanol, which had values of Ω_R equal to 0.58 and 0.90, respectively, after the test. Values of Ω_R were corrected for this loss by assuming all water displaced by deployment and retrieval of a sorbent column is forced through the sorbent matrix; hence, this volume of water is subtracted from the cumulative water flux q_0t given by tracers alone. Nonetheless, water fluxes calculated for experiments using the residual masses of methanol and ethanol yielded unsatisfactory results.

Additionally, it has been shown previously that estimates of q_0 are most accurate for a range of residual tracer masses around Ω_R

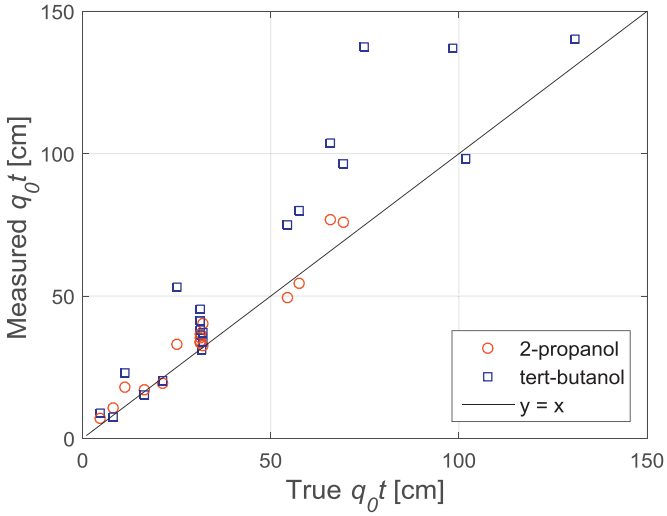

Fig. 6. Measured versus true cumulative water fluxes.

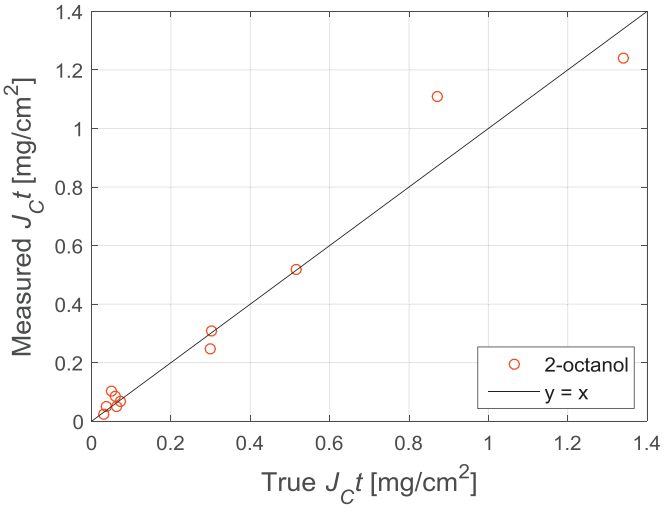

Fig. 7. Measured versus true cumulative 2-octanol mass flux.

≈ 0.5 (Hatfield et al., 2004). For any given tracer, there is a specific range of cumulative water fluxes that will yield acceptable values of Ω_R and lead to accurate estimates of q_0 based on SBPFM geometry and the retardation factor of the tracer. Short periods of SBPFM deployment resulted in values of Ω_R that were too high for accurate results using tracers of high retardation. On the other hand, longer tests resulted in inaccurate estimates of q_0 when considering tracers with low retardation factors, which is likely exacerbated by additional elution during installation and retrieval. Several tests were conducted to determine if methanol and ethanol could accurately predict smaller cumulative fluxes but results were inconsistent, likely a result of elution during installation and retrieval. Estimates of fluxes using tert-butanol were acceptable for some trials but generally had values of Ω_R too high for generating accurate results, indicating that this tracer may be more effective for measuring higher water fluxes or for longer deployment durations.

4.2. Cumulative water and contaminant mass fluxes

Measured cumulative water fluxes based on 2-propanol and tert-butanol are compared to true cumulative water fluxes as determined in Appendix B3 (Fig. 6). Of the resident tracers used, 2-propanol produced the most accurate estimates of cumulative water flux. Relative errors for estimates of cumulative ambient specific discharge by tracers 2-propanol and tert-butanol were found to be 16% ± 18% (mean ± standard deviation) and 24% ± 35%, respectively. Estimated cumulative 2-octanol mass fluxes through the sediment are also compared to their true counterparts (Fig. 7). True cumulative contaminant mass fluxes were calculated from the concentration of 2-octanol in the water being supplied to the sediment bed simulator and the ambient specific discharge in the sediment bed as $J_C = q_0 c_F$, where q_0 was determined as described in Appendix B3. Relative errors in estimates of cumulative 2-octanol mass flux were found to be 13% ± 35%.

Due to the volatile nature of the 2-octanol in solution and the airflow across the surface of the water column on top of the sediment bed simulator, effluent concentrations ranged from 24% to 76% of the initial concentration. Consequently, verification of results by contaminant mass balance calculation between bucket inflow, outflow and SBPFM retention was not possible. However, because the influent was not exposed to airflow until exiting the sediment layer at the top, it was assumed that volatilization had no impact on the mass flux through the sediment to be measured.

4.3. Diffusion and non-equilibrium sorption

Eqs. (8) and (9) are based on the assumptions of advection dominated transport and instantaneous (equilibrium) sorption in the SBPFM. While diffusive losses of tracers from the sorbent column may lead to overestimation of water fluxes, non-equilibrium desorption of tracers may decrease the efficiency of tracer elution and cause underestimation of water fluxes. In contrast, for contaminant fluxes, both diffusive losses and non-equilibrium sorption have the potential to negatively impact m_C and, hence, cause underestimation of contaminant fluxes. Following Hatfield et al. (2004), we evaluate the relative importance of diffusion versus advection using the Peclet number *Pe* [-] defined as

$$Pe = \frac{q_c L_c}{\theta^{7/3} D} \tag{17}$$

where D [L^2/T] is the aqueous diffusion coefficient for a tracer or contaminant, which we assume to be on the order of 1 cm^2/d (Hatfield et al., 2004). With $L_c \approx 10$ cm and $\theta \approx 0.5$ this leads to the condition of $q_c > 0.2$ cm/d for safely neglecting diffusive transport, i.e., $Pe > 10$ in the sorbent column. For expected values of α_q on the order of 1 to 10 in practice, this value of 0.2 cm/d may also be regarded as a conservative lower limit for the undisturbed sediment flux q_0. Our current test results are limited to $q_0 \geq 14$ cm/d and $\alpha_q \approx 3$, i.e., approximately $q_c > 50$ cm/d, which is within the advection dominated range.

Also following Hatfield et al. (2004), we evaluate the relative importance of sorption kinetic rate versus advective transport rate using the Damkohler number *Da* [-] defined as

$$Da = \frac{kR_d(1-\beta)L_c}{q_c} \tag{18}$$

where k [1/T] is the tracer or contaminant (de)sorption rate coefficient and β [-] is the fraction of sorption sites, where equilibrium sorption is assumed. Taking k to be on the order of 1 1/h and $\beta \approx 0.5$ (Hatfield et al., 2004) and using $R_d \approx 100$ (e.g., 2-propanol; Table 1), we arrive at the condition $q_c < 1200$ cm/d for safely neglecting non-equilibrium sorption, i.e., $Da > 10$ in the sorbent column. For a large assumed value of $\alpha_q \approx 10$, this translates into the conservative condition of $q_0 < 120$ cm/d. Our current test results are for maximum values of $\alpha_q \approx 6$ and limited to $q_0 \leq 242$ cm/d, i.e., approximately $q_c < 1500$ cm/d, which is within the equilibrium range or near its limit. Overall, this shows that SBPFM application based on the present assumptions of advection dominated trans-

port and instantaneous sorption is appropriate for a range of vertical sediment fluxes q_0 between mm/d (diffusion limit) and m/d (non-equilibrium limit). Eqs. (17) and (18) show that increasing L_c and/or R_d by using longer columns and/or more hydrophobic tracers may further expand this range.

4.4. Non-linear and competitive sorption

While Eq. (9) for estimating contaminant mass flux is based on the assumption that intercepted contaminants are fully sorbed and do not degrade or exit the sorbent column, Eq. (8) for estimating water flux is based on the assumption of linear tracer desorption, i.e., a constant value of retardation factor R_d for each tracer. As discussed in Section 3.2.3, values of R_d were determined from independent tracer elution experiments using sorbent columns under conditions similar to the SBPFM experiments. Results for such column elution experiments have been published previously for different flux meter applications (Hatfield et al., 2004; Annable et al., 2005; Klammler et al., 2016). Even for strongly non-linear sorption isotherms, column elution curves can be expected to be initially linear over significant ranges due to the uniform initial distribution of tracers on the sorbent in the column. For the present experiments, this was found to be the case for $\Omega_R > 0.3$, which was applied as a criterion for data interpretation. However, if necessary, this limitation may be overcome by superimposing multiple linear elution functions to generate an approximation of a non-linear elution function (Hatfield et al., 2004).

Tracer column elution tests were performed using the same mix of tracers as for SBPFM experiments. Thus, resulting retardation factors inherently account for the possibility of competitive sorption between tracers. Competitive sorption between tracers and contaminants is not expected to influence results, because the initial portion of the sorbent column retaining the contaminants is already void of tracers (retardation is generally much larger for contaminants than for tracers). Competitive sorption between different contaminants needs to be evaluated on a case-by-case basis, but is not an issue in practice as long as contaminants are fully retained. In combination with the other assumptions of Section 3.1.2, this assures applicability of Eq. (9), which does not require a contaminant retardation factor.

4.5. Tracer release, flow direction and contaminant retention

During SBPFM deployment, the sorbent column releases tracers into the sediment bed. However, due to the non-toxic nature of the tracers (short-chain alcohols) and the small amounts released (< 1 g), obtaining approval for different types of passive flux meter applications in groundwater has not been a problem (e.g., Brooks et al., 2008; Verreydt et al., 2013; Wang et al., 2014). Tracer release from the SBPFM can be completely avoided, if only the center portion of the sorbent column is initially impregnated with tracers, while the extreme portions are not and retain tracers after displacement. Analyzing the center portion separately for tracer mass remaining, then allows quantification of water flux as described here. Also analyzing the extreme portions for displaced tracer mass, further allows distinguishing upward or downward flow direction. Horizontal flow components in the sediment bed are not expected to affect measurements of vertical fluxes, as they do not cause flow through the sorbent column located in the center of the SBPFM.

Technically, contaminant mass fluxes can be measured for most organic and inorganic compounds by selecting the appropriate type or mix of sorbent materials to be employed in the SBPFM column. For example, granular activated carbon (GAC) and activated carbon felt (AC-felt) have been used for volatile organic compounds (VOCs) like perchloroethylene, trichloroethylene, benzene, toluene, MTBE, naphthalene, etc. For semi-volatile organic compounds (SVOCs) including polycyclic aromatic hydrocarbons (PAHs), and RDX, non-ionic resins have been employed. For heavy metals (Cr, As, U, etc.), and ionic compounds (Cl, Br, phosphate, nitrate, ammonium, perchlorate etc.) anionic and cationic resins have been used (Cho et al., 2007; Lee et al., 2007). Other suitable sorbents include zeolites and aluminum oxides (Clark et al., 2005).

5. Summary

The sediment bed passive flux meter (SBPFM) is a new device for providing simultaneous point measurements of cumulative vertical water and contaminant mass fluxes in lake or stream sediment beds. It is a self-contained passive permeable unit that may be driven directly into the sediment bed for deployment periods ranging from hours to weeks. The device is designed to contain a permeable matrix of hydrophobic and/or hydrophilic sorbents, which passively intercept ambient flow through the sediment bed resulting from surface and groundwater interactions. The sorbents release resident tracers at rates proportional to groundwater flux and retain dissolved contaminants from groundwater at rates proportional to contaminant mass flux. Prior knowledge of the water flux is not required because several resident tracers are used with varying retardation factors. Flow direction may be inferred by segmented analysis of the sorbent column, revealing the direction of tracer displacement and/or the direction of contaminant arrival. All flux estimates are time-cumulative, thus effectively integrating (or averaging) temporal fluctuations in both water flux and contaminant concentrations during deployment periods.

In the present work, we develop relationships between fluxes measured through SBPFM sorbents and undisturbed ambient fluxes through the sediment bed. In order to demonstrate the fundamental working principle and validate the theory, multiple experiments were conducted using a bench-scale sediment bed simulator with granular activated carbon as a sorbent. Cumulative groundwater flux was quantified using a suite of four alcohol tracers, of which 2-propanol and tert-butanol provided satisfactory results. Estimates of cumulative water flux made using tracers methanol and ethanol were not reflective of the true flux, because lower retardation led to significant elution during installation and retrieval of the SBPFM. 2-octanol served as a surrogate contaminant in these bench-scale experiments and estimates of respective mass fluxes were also satisfactory.

Moving SBPFM to the field is certain to pose several challenges. For example, the flow convergence factor α_q depends on the hydraulic conductivities in the horizontal and vertical directions, which are challenging to measure. However, a number of approaches for solving this problem appears possible (Klammler et al., under review in AWR as manuscript ADWR_2016_360_R1). Furthermore, we identify a range of conditions, over which knowledge of vertical conductivity suffices (Fig. 4) and propose a simple field method for its measurement. Finally, the current testing of the SBPFM did not include flow reversal in the sediment bed as, for example, associated with tidally influenced streams or lakes.

Acknowledgments

This work was partially funded by the Florida Water Resources Research Center under a grant from the U.S. Department of Interior U.S. Geological Survey (G11AP20072) and by CH2M Hill through a donation to the Engineering School of Sustainable Infrastructure and Environment at the University of Florida.

Appendix A. Flow convergence coefficient α_q

Darcy's law for one-dimensional flow through the sorbent column Q_c [L^3T^{-1}] is

$$Q_c = \frac{\Delta\phi K_c r_c^2 \pi}{L_c} \tag{A1}$$

where $\Delta\phi$ [L] is the head difference across the column. Imagine the SBPFM is exposed to a vertical gradient J [-] in a sediment while leaving the SBPFM "open" (i.e., $K_c = \infty$). The volumetric flow rate through the open SBPFM Q_{open} [L^3T^{-1}] is written as

$$Q_{open} = F_{open} K_v J a^2 \pi \tag{A2}$$

where F_{open} serves as a proportionality constant between Q_{open} and the undisturbed sediment discharge $K_v J a^2 \pi$ through a horizontal cross sectional area of the SBPFM. Next, consider the scenario of $J = 0$ and application of a discharge Q_{rec} [L^3T^{-1}] between the two screens. This corresponds to recirculating flow between screens (e.g., using a hypothetical pump) and is written

$$Q_{rec} = F_{rec} \frac{\Delta\phi K_v a^2 \pi}{p + s} \tag{A3}$$

where F_{rec} [-] is a proportionality constant between Q_{rec} and the discharge $\Delta\phi K_v a^2 \pi/(p+s)$ through a sediment column equal in size to the probe between screen centers causing a head drop $\Delta\phi$.

The expressions of Eqs. (A2) and (A3) can be superimposed to find a solution for $J > 0$ and $K_c < \infty$, as it is the general SBPFM scenario. This does not affect the correct solution of an undisturbed hydraulic gradient far from the screens (or at nearby boundaries of the flow domain), while it imposes a non-zero head difference between the screens. Because $K_c < \infty$ hinders flow through the SBPFM, the flow through the column is $Q_c = Q_{open} - Q_{rec}$. Substituting Eq. (A3) and eliminating $\Delta\phi$ using Eq. (A1) then gives

$$\frac{Q_c}{Q_{open}} = \frac{1}{1 + \frac{a^2 L_c K_v}{r_c^2 (p+s) K_c} F_{rec}} \tag{A4}$$

which relates Q_c to Q_{open} for arbitrary values of K_c and independent of J. Substituting Eq. (A2) with $JK_v = q_0$ and knowing $Q_c = q_c r_c^2 \pi$ yields Eq. (10), with F_{open} and F_{rec} derived in Appendix B.

Appendix B. Shape factors

The constants F_{open} and F_{rec} are determined following the method described by Klammler et al. (2011) for a homogenous saturated sediment bed (Fig. B1). Variables r and z denote the radial and vertical coordinates, respectively, and are delimited by $a < r < b$ and $0 < z < d$, where b [L] is the radial distance to the lateral boundary (I) and d [L] is the distance between top (II) and bottom (III) boundaries. Lateral boundary (I) is considered impermeable, while boundaries (II) and (III) are at constant heads. This is consistent with the possibility of a uniform vertical gradient over the flow domain. Internal boundaries along the SBPFM are delimited by h_1 through h_4 [L]. Boundaries (IV), (VI) and (VIII) are impermeable, while boundaries (V) and (VII) are at constant heads. Distance d_{bot} [L] is the length of impermeable boundary (IV) and d_{top} [L] is the length of impermeable boundary (VIII).

The governing Laplace equation for steady-state flow and isotropic hydraulic conductivity in cylindrical coordinates is

$$\frac{\partial^2\phi(r,z)}{\partial r^2} + \frac{1}{r}\frac{\partial\phi(r,z)}{\partial r} + \frac{\partial^2\phi(r,z)}{\partial z^2} = 0 \tag{B1}$$

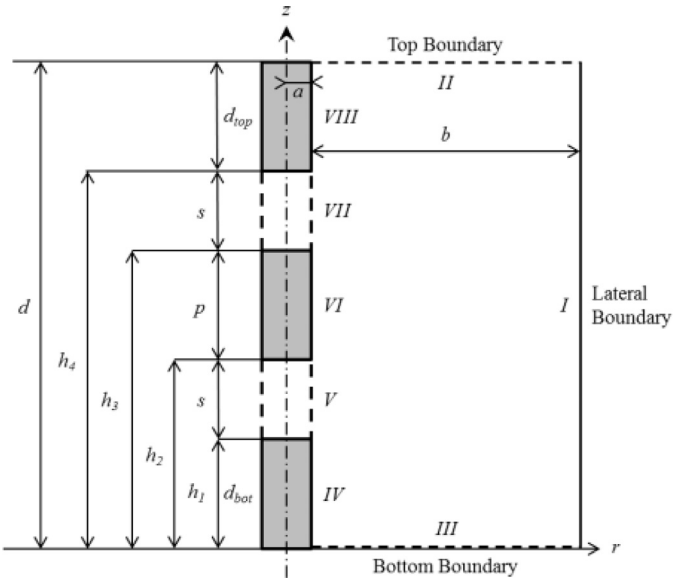

Fig. B1. Schematic of axisymmetric flow domain and boundary conditions. Impermeable boundaries are bold continuous and constant head boundaries are bold dashed.

where $\phi(r, z)$ [L] is the hydraulic head distribution within the flow domain. A general solution of Eq. (B1) is (Zaslavsky and Kirkham, 1964)

$$\begin{aligned}\phi(r,z) = {} & [c_1\sin(m_1 z) + c_2\cos(m_1 z)][c_3 I_0(m_1 r) + c_4 K_0(m_1 r)] \\ & + [c_5\sinh(m_2 z) + c_6\cosh(m_2 z)][c_7 J_0(m_2 r) + c_8 Y_0(m_2 r)] \\ & + c_9 z\ln(r/m_3) + c_{10}\ln(r/m_3) + c_{11} z + c_{12}\end{aligned} \tag{B2}$$

where J_0, Y_0, I_0, and K_0 are Bessel functions of order zero (Dwight, 1947), and where c_i for $i = 1,2,\ldots,12$ and m_j for $j = 1,2,3$ are arbitrary real constants (m_j being positive). The three external boundary conditions (I)–(III) can be mathematically expressed as

I)

$$\frac{\partial\phi}{\partial r} = 0 \quad \text{at } r = b \text{ for } 0 \le z \le d \tag{B3}$$

II)

$$\phi(r,z) = \phi_{II} \text{ at } z = d \text{ for } a \le r \le b \tag{B4}$$

III)

$$\phi(r,z) = \phi_{III} \text{ at } z = 0 \text{ for } a \le r \le b \tag{B5}$$

To represent constant head top (II) and bottom (III) boundaries at different heads, we discard incompatible terms of the general solution in Eq. (B1), while superimposing compatible terms, leading to

$$\phi(r,z) = c_{11} z + c_{12} + \sum_{n=1}^{N} B_n f_0(mr)\sin(mz) \tag{B6}$$

where $m = n\pi/d$, n and N are positive integers, B_n are a new set of constants encompassing c_1, c_2, and c_4, while $f_0(mr)$ is a function to be defined involving terms of the equation that contain the Bessel functions K_0 and I_0. For an impermeable lateral boundary, the function $f_0(mr)$ is expressed as (Klammler et al., 2011)

$$f_0(mr) = \frac{\frac{K_0(mr)}{K_1(mb)} + \frac{I_0(mr)}{I_1(mb)}}{\frac{K_1(ma)}{K_1(mb)} - \frac{I_1(ma)}{I_1(mb)}} \tag{B7}$$

where K_1 and I_1 are Bessel functions of the first order (Dwight, 1947). Under field conditions, where the lateral impermeable

boundary is located far away from the SBPFM ($b >> a$), $f_0(mr)$ reduces to

$$f_0(mr) = \frac{K_0(mr)}{K_1(ma)} \tag{B8}$$

The values of the coefficients B_n in Eq. (B6) do not affect compliance with external boundary conditions (I), (II), and (III). Thus, these coefficients may be used to independently meet the internal (mixed) boundary conditions (IV)–(VIII) expressed as

IV)

$$\frac{\partial \phi}{\partial r}|_{r=a} = 0 \text{ for } 0 \le z < h_1 \tag{B9}$$

V)

$$\phi(a,z) \phi_V \text{ for } h_1 \le z \le h_2 \tag{B10}$$

VI)

$$\frac{\partial \phi}{\partial r}|_{r=a} = 0 \text{ for } h_2 \le z < h_3 \tag{B11}$$

VII)

$$\phi(a,z) = \phi_{VII} \text{ for } h_3 \le z \le h_4 \tag{B12}$$

VIII)

$$\frac{\partial \phi}{\partial r}|_{r=a} = 0 \text{ for } h_4 \le z \le d \tag{B13}$$

where ϕ_V and ϕ_{VII} [L] are the constant hydraulic heads in the bottom and top screen, respectively. The solution for $\phi(a,z)$ of Eq. (B6) is substituted into equations (B9)–(B13), where $c_{12} = \phi_{III}$ is arbitrarily set to zero and $c_{11} = J$ is identified as the vertical hydraulic gradient. This results in the following system of equations representing the internal boundary conditions:

IV)

$$\sum_{n=1}^{N} B_n \frac{n\pi}{d} \sin(mz_i) = 0 \text{ for } 0 \le z_i < h_1 \tag{B14}$$

V)

$$Jz_i + \sum_{n=1}^{N} B_n f_0(ma) \sin(mz_i) = \phi_V \text{ for } h_1 \le z_i < h_2 \tag{B15}$$

VI)

$$\sum_{n=1}^{N} B_n \frac{n\pi}{d} \sin(mz_i) = 0 \text{ for } h_2 \le z_i < h_3 \tag{B16}$$

VII)

$$Jz_i + \sum_{n=1}^{N} B_n f_0(ma) \sin(mz_i) = \phi_{VII} \text{ for } h_3 \le z_i < h_4 \tag{B17}$$

VIII)

$$\sum_{n=1}^{N} B_n \frac{n\pi}{d} \sin(mz_i) = 0 \text{ for } h_4 \le z_i \le d \tag{B18}$$

where $K_0(r)/dr = -K_1(r)$ and $I_0(r)/dr = I_1(r)$, leading to $df_0(mr)/dr|_{r=a} = -m$, was used. In the above system of equations, following Klammler et al. (2011), the device length $0 \le z \le d$ is discretized into equidistant control points z_i such that $z_1 = d/(2N)$ and $z_i = z_{i-1} + d/N$ for i=1,2,...,*N*. Equations (B14)–(B18) represent a linear system of *N* equations with $N+2$ unknown coefficients (B_n, ϕ_V and ϕ_{VII}), which imposes the required boundary conditions at the control points.

Appendix B1. Shape factor F_{open} for flow through the open SBPFM

For open flow through the column of the SBPFM ($K_c = \infty$), the hydraulic heads at the top and bottom screens are still unknown but equal such that $\phi_V = \phi_{VII}$ provides one additional equation. Imposing continuity of flow between both screens as

$$Q_V + Q_{VII} = 0 \tag{B19}$$

provides the second equation, where Q_V and Q_{VII} [L^3T^{-1}] are the volumetric flow rates through the internal boundaries (V) and (VII), respectively. These flow rates can be expressed as

$$\begin{aligned} Q_V &= -2\pi aK \int_{h_1}^{h_2} \left. \frac{\partial \phi}{\partial r} \right|_{r=a} dz \\ &= 2\pi aK \sum_{n=1}^{N} B_n [\cos(mh_2) - \cos(mh_1)] \end{aligned} \tag{B20}$$

$$\begin{aligned} Q_{VII} &= -2\pi aK \int_{h_3}^{h_4} \left. \frac{\partial \phi}{\partial r} \right|_{r=a} dz \\ &= 2\pi aK \sum_{n=1}^{N} B_n [\cos(mh_4) - \cos(mh_3)] \end{aligned} \tag{B21}$$

leading to

$$\sum_{n=1}^{N} B_n \langle [\cos(mh_2) - \cos(mh_1)] + [\cos(mh_4) - \cos(mh_3)] \rangle = 0 \tag{B22}$$

as the last condition required. After dividing the system by $\phi_{II} = Jd$ the coefficients B_n/ϕ_{II} can be found. Subsequently, F_{open} is found by combining Eq. (A2) with $J = \phi_{II}/d$ and (B20) to form

$$F_{open} = 2\frac{d}{a} \sum_{n=1}^{N} \frac{B_n}{\phi_{II}} \left[\cos\left(n\pi \frac{h_2}{d} \right) - \cos\left(n\pi \frac{h_1}{d} \right) \right] \tag{B23}$$

Under anisotropic conditions of horizontal and vertical hydraulic conductivities K_H and K_V, it is known that above results remain valid if all radial distances of the sediment flow domain (i.e., *r*, *a* and *b*) are multiplied by ρ, while maintaining the vertical coordinates unchanged (Hvorslev, 1951). With this, Eq. (B23) can be graphically represented for field conditions of anisotropic conductivity, distant lateral boundaries ($b >> a$) using Eq. (B8) and distant bottom boundary ($d_{bot}/s = 50$; Fig. 2). The graphs are shown for $d_{top}/s = 1$ and were found to be accurate (visually indistinguishable) for the entire range of $d_{top}/s > 0.5$. This implies a large degree of robustness with respect to the distance between SBPFM screens and the groundwater–surface water interface (i.e., nearby top boundary).

Appendix B2. Shape factor F_{rec} for recirculating flow through SBPFM

In the case of recirculating flow in the absence of an ambient gradient ($J = 0$) the screen heads ϕ_V and ϕ_{VII} are unequal. Besides equations (B14)–(B18), two additional equations are formed by setting Q_V and $-Q_{VII}$ equal to recirculation flow Q_{rec} in equations (B20) and (B21), resulting in

$$Q_{rec} = 2\pi aK \sum_{n=1}^{N} B_n [\cos(mh_2) - \cos(mh_1)] \tag{B24}$$

$$Q_{rec} = -2\pi aK \sum_{n=1}^{N} B_n [\cos(mh_4) - \cos(mh_3)] \tag{B25}$$

for the isotropic scenario. The coefficients $B_n aK/Q_{rec}$ are found from solving the linear system of equations (B14)–(B18) with equations (B24) and (B25). Subsequently, $\Delta\phi aK/Q_{rec} = (\phi_V - \phi_{VII})aK/Q_{rec}$ may be expressed from equations (B15) and (B17), remembering $J = 0$, and substituted into Eq. (A3) to find F_{rec} as

$$F_{rec} = \frac{\frac{s}{a\pi}\left(1+\frac{p}{s}\right)}{\sum_{n=1}^{N}\frac{B_n aK}{Q_{rec}} f_0\left(n\pi\frac{a}{d}\right)\left[\sin\left(n\pi\frac{h_1}{d}\right)-\sin\left(n\pi\frac{h_3}{d}\right)\right]} \quad \text{(B26)}$$

A generalization to anisotropic conditions is again straightforward and accomplished by multiplying all radial distances by ρ, while substituting K_H for K to assure continuity of flow (Hvorslev, 1951). With this, Eq. (B26) can be graphically represented as F_{open}/F_{rec} for field conditions of anisotropic conductivity as well as distant bottom and lateral boundaries (using $d_{bot}/s = 50$ and Eq. (B8); Fig. 3). Graphs of Eq. (B26) are again for $d_{top}/s = 1$ being accurate (visually indistinguishable) for the entire range of $d_{top}/s > 0.5$.

Appendix B3. Application to the sediment bed simulator

For the configuration of the sediment bed simulator, the constants F_{open} and F_{rec} are found as in Appendices B1 and B2, where Eq. (B7) with $b = 14$ cm is used instead of Eq. (B8). Thus, equations (8)–(10) remain valid if, according to Eq. (A2), q_0 and J_C are interpreted as the uniform vertical fluxes through the sediment in the absence of the SBPFM (or, equivalently, with both of its screens closed). However, it is obvious that during the experiments the SBPFM is present and hydraulically active, such that q_0 and J_C cannot be directly observed for validation of measured fluxes. Instead, we may observe the total flow Q_{sim} through the simulator and compute the flux $q_{sim} = Q_{sim}/[\pi(b^2 - a^2)]$, where

$$Q_{sim} = -2\pi K\int_a^b \left.\frac{\partial\phi}{\partial z}\right|_{z=0} rdr = q_0\pi\left(b^2-a^2\right)+2\pi aK\sum_{n=1}^{N}B_n \quad \text{(B27)}$$

is obtained from integrating the vertical fluxes across the bottom boundary. The coefficients B_n are hereby found from the system of equations (B14)–(B18) with Eq. (B22) establishing continuity of flow and

$$K_c r_c^2\frac{\phi_{VII}-\phi_V}{L_c} = 2aK\sum_{n=1}^{N}B_n[\cos(mh_2) - \cos(mh_1)] \quad \text{(B28)}$$

imposing Darcy's law across the sorbent column. After solving the resulting system of equations for B_n/ϕ_{II}, we compute

$$\frac{q_{sim}}{q_0} = 1+\frac{2d}{a\left(\frac{b^2}{a^2}-1\right)}\sum_{n=1}^{N}\frac{B_n}{\phi_{II}} = 1.05 \quad \text{(B29)}$$

where it is remembered that under anisotropic conditions $a\rho$, $b\rho$ and K_H are to be used instead of a, b, and K for finding B_n/ϕ_{II} and in Eq. (B29). Note that r_c is not scaled due to anisotropy. With this, the true fluxes (Fig. 6) are obtained by dividing the independently observed sediment bed simulator fluxes q_{sim} by Eq. (B29). The same correction is performed for true mass fluxes (Fig. 7). Under field conditions, this correction becomes irrelevant, since $b/a >> 1$ and $q_{sim}/q_0 \approx 1$.

Appendix C. Anisotropy and horizontal hydraulic conductivity using bucket injection test

When simultaneously injecting through both screens using a known injection head ϕ_{inj} [L], equations (B14)–(B18) remain valid with $J = 0$ and $\phi_V = \phi_{VII} = \phi_{inj}$. Anisotropic conditions (i.e., $\rho \neq 1$) can be accounted for by multiplying all radial distances (i.e., a and b in the present case) by ρ (Hvorslev, 1951). After dividing the resulting system of N equations and N unknowns by ϕ_{inj}, the coefficients B_n/ϕ_{inj} can be solved for. The steady-state injection flow Q_{inj} [L^3T^{-1}] is measured during the injection test, and for anisotropic conditions can be expressed as

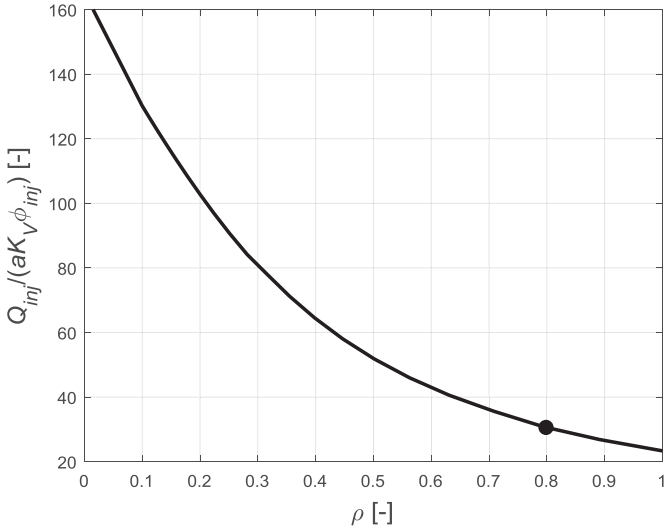

Fig. C1. $Q_{inj}/(aK_v\phi_{inj})$ for injected flow through SBPFM as a function of ρ for sediment bed simulator configuration. A known value of $Q_{inj}/(aK_v\phi_{inj}) = 31$ leads to $\rho = 0.8$ as indicated by the dot.

$$Q_{inj} = -2\pi a\rho K_H\int_0^d \left.\frac{\partial\phi}{\partial r}\right|_{r=a\rho} dz \quad \text{(C1)}$$

where K_H is used to assure continuity of flows between anisotropic and scaled isotropic flow domains (Hvorslev, 1951). Using Eqs. (11) and (B24) with $h_1 = 0$ and $h_2 = d$, Eq. (C1) can be rearranged into

$$\frac{Q_{inj}}{aK_V\phi_{inj}} = \frac{2\pi}{\rho}\sum_{n=1}^{N}\frac{B_n}{\phi_{inj}}[\cos(n\pi)-1] \quad \text{(C2)}$$

The left-hand-side of Eq. (C2) is plotted as a function of ρ (Fig. C1) for the geometry of the sediment bed simulator, noting that B_n/ϕ_{inj} are also functions of ρ through equations (B14)–(B18). By knowing $a = 2.1$ cm, $\phi_{inj} = 1.0$ cm and $Q_{inj} = 0.44$ m^3/d from the injection test performed, as well as $K_V = 68.5$ m/d from the constant head vertical flow test, $Q_{inj}/(aK_v\phi_{inj}) = 31$ leads to $\rho = 0.8$ (Fig. C1).

References

Annable, M., Hatfield, K., Cho, J., Klammler, H., Parker, B., Cherry, J., Rao, P.S.C., 2005. Field-scale evaluation of the passive flux meter for simultaneous measurement of groundwater and contaminant fluxes. Environ. Sci. Technol. 39, 7194–7201.

Baxter, C., Hauer, F.R., Woessner, W.W., 2003. Measuring groundwater–stream water exchange: new techniques for installing minipiezometers and estimating hydraulic conductivity. Trans. Am. Fish. Soc. 132 (3), 493–502.

Bear, J., 2013. Dynamics of Fluids in Porous Media. Courier Corporation.

Belanger, T., Montgomery, M., 1992. Seepage meter errors. Limnol. Oceanogr. 37 (8), 1787–1795.

Boano, F., Revelli, R., Ridolfi, L., 2007. Bedform-induced hyporheic exchange with unsteady flows. Adv. Water Resour. 30 (1), 148–156.

Boulton, A.J., Findlay, S., Marmonier, P., Stanley, E.H., Valett, H.M., 1998. The functional significance of the hyporheic zone in streams and rivers. Annu.Rev. Ecol. Syst. 59–81.

Brooks, M.C., Wood, A.L., Annable, M.D., Hatfield, K., Cho, J., Holbert, C., Rao, P.S.C., Enfield, C.G., Lynch, K., Smith, R.E., 2008. Changes in contaminant mass discharge from DNAPL source mass depletion: evaluation at two field sites. J. Contam. Hydrol. 102, 140–153.

Brodie, R., Baskaran, S., Ransley, T., Spring, J., 2009. Seepage meter: progressing a simple method of directly measuring water flow between surface water and groundwater systems. Aust. J. Earth Sci. 56 (1), 3–11.

Bufflap, S.E., Allen, H.E., 1995. Sediment pore water collection methods for trace metal analysis: a review. Water Res. 29 (1), 165–177.

Cho, J., Annable, M.D., Jawitz, J.W., Hatfield, K., 2007. Passive flux meter measurement of water and nutrient flux in porous media. J. Environ. Qual. 36, 1266–1272.

Clark, C.J., Hatfield, K., Annable, M.D., Gupta, P., Chirenje, T., 2005. Estimation of arsenic contamination in groundwater by the passive flux meter. Environ. Forensics 6, 77–82.
Constantz, J., Stonestorm, D., Stewart, A.E., Niswonger, R., Smith, T.R., 2001. Analysis of streambed temperatures in ephemeral channels to determine streamflow frequency and duration. Water Resour. Res. 37 (2), 317–328.
Dwight, H.B., 1947. Tables of Integrals and Other Mathematical Data. The MacMillan Company, New York.
Ghosh, U., et al., 2014. Passive sampling methods for contaminated sediments: practical guidance for selection, calibration, and implementation. Integr. Environ. Assess. Manage. 10 (2), 210–223.
Hatfield, K., Annable, M., Cho, J., Rao, P.S.C., Klammler, H., 2004. A direct passive method for measuring water and contaminant fluxes in porous media. J. Contam. Hydrol. 75 (3–4), 155–181.
Hvorslev, M.J., 1951. Time lag and soil permeability in groundwater observations. Bulletin No. 36. U.S. Army Corps of Engineers, Vicksburg, Mississippi.
Kalbus, E., Reinstorf, F., Schirmer, M., 2006. Measuring methods for groundwater–surface water interactions: a review. Hydrol. Earth Syst. Sci. 10 (6), 873–887.
Klammler, H., Hatfield, K., Nemer, B., Mathias, S.A., 2011. A trigonometric interpolation approach to mixed type boundary problems associated with permeameter shape factors. Water Resour. Res. 47 (3).
Klammler, H., Hatfield, K., Newman, M., Cho, J., Annable, M., Parker, B., Cherry, J., Perminova, I., 2016. A new device for characterizing fracture networks and measuring groundwater and contaminant fluxes in fractured rock aquifers. Water Resour. Res. 52, WR018389.
Lee, D.R., 1977. A device for measuring seepage flux in lakes and esturies. Limnol. Oceanogr. 22 (1), 140–147.
Lee, J., Rao, P.S.C., Poyer, I.C., Toole, R.M., Annable, M.D., Hatfield, K., 2007. Oxyanion flux characterization using passive flux meters: development and field testing of surfactant-modified sorbents. J. Contam. Hydrol. 92 (3-4), 208–229.
Murdoch, L.C., Kelly, S.E., 2003. Factors affecting the performance of conventional seepage meters. Water Resour. Res. 39 (6).
Packman, A.I., Salehin, M., 2003. Relative roles of stream flow and sedimentary conditions in controlling hyporheic exchange. In: The Interactions Between Sediments and Water. Springer, pp. 291–297.
Rosenberry, D.O., 2008. A seepage meter designed for use in flowing water. J. Hydrol. 359 (1), 118–130.
Rosenberry, D.O., Morin, R.H., 2004. Use of an electromagnetic seepage meter to investigate temporal variability in lake seepage. Groundwater 42 (1), 68–77.
Russoniello, C.J., Michael, H.A., 2014. Investigation of seepage meter measurements in steady flow and wave conditions. Groundwater 53 (6), 959–966.
Sawyer, A.H., Lazareva, O., Koreger, K.D., Crespo, K., Chan, C.S., Stieglitz, T., Michael, H.A., 2014. Stratigraphic controls on fluid and solute fluxes across the sediment–water interface of an estuary. Limnol. Oceanogr. 59 (3), 997–1010.
Taniguchi, M., Fukuo, Y., 1993. Continuous measurements of ground-water seepage using an automatic seepage meter. Groundwater 31 (4), 675–679.
Verreydt, G., Annable, M.D., Kaskassian, S., Van Keer, I., Bronders, J., Diels, L., Vanderauwera, P., 2013. Field demonstration and evaluation of the passive flux meter on a CAH groundwater plume. Environ. Sci. Pollut. Res. 20 (7), 4621–4634.
Vrana, B., Allan, I.J., Greenwood, R., Mills, G.A., Dominiak, E., Svensson, K., Knutsson, J., Morrison, G., 2005. Passive sampling techniques for monitoring pollutants in water. TrAC Trends Anal. Chem. 24 (10), 845–868.
Wang, F., Annable, M.D., Schaefer, C.F., Ault, T.D., Cho, J., Jawitz, J.W., 2014. Enhanced aqueous dissolution of a DNAPL source to characterize the source strength function. J. Contam. Hydrol. 169, 75–89.
Winter, T.C., Harvey, J.W., Franke, O.L., Alley, W.W., 1998. Ground water and surface water: a single resource. U.S. Geol. Surv. Circ. 1139, 79.
Winter, T.C., 2001. Ground water and surface water: the linkage tightens, but challenges remain. Hydrol. Processes 15 (18), 3605–3606.
Zaslavsky, D., Kirkham, D., 1964. The streamline function for axially symmetric groundwater movement. Soil Sci. Soc. Am. J. 28 (2), 156–160.